Variational determination of approximate bright matter-wave soliton solutions in anisotropic traps

T. P. Billam, S. A. Wrathmall, and S. A. Gardiner
Department of Physics, Durham University, Durham DH1 3LE, United Kingdom
(Received 29 November 2011; published 19 January 2012)

We consider the ground state of an attractively interacting atomic Bose-Einstein condensate in a prolate, cylindrically symmetric harmonic trap. If a true quasi-one-dimensional limit is realized, then for sufficiently weak axial trapping this ground state takes the form of a bright soliton solution of the nonlinear Schrödinger equation. Using analytic variational and highly accurate numerical solutions of the Gross-Pitaevskii equation, we systematically and quantitatively assess how solitonlike this ground state is, over a wide range of trap and interaction strengths. Our analysis reveals that the regime in which the ground state is highly solitonlike is significantly restricted and occurs only for experimentally challenging trap anisotropies. This result and our broader identification of regimes in which the ground state is well approximated by our simple analytic variational solution are relevant to a range of potential experiments involving attractively interacting Bose-Einstein condensates.

DOI: 10.1103/PhysRevA.85.013627 PACS number(s): 03.75.Lm, 67.85.Bc

I. INTRODUCTION

Bright solitons are self-focusing, nondispersive, particlelike solitary waves occurring in integrable systems [1,2]. They behave in a particlelike manner, emerging from mutual collisions intact except for shifts in their position and relative phase. Bright soliton solutions of the one-dimensional nonlinear Schrödinger equation (NLSE) can be described analytically using the inverse-scattering technique [3,4] and are well known in the context of focusing nonlinearities in optical fibers [4,5]. Bright solitary matter waves in an attractively interacting atomic Bose-Einstein condensate (BEC) represent an intriguing alternative physical realization [6–8]. In a mean-field description an atomic BEC obeys the Gross-Pitaevskii equation (GPE) [9], a three-dimensional NLSE. While in general nonintegrable, in a homogeneous, quasi-one-dimensional (quasi-1D) limit the GPE reduces to the one-dimensional NLSE, thus supporting bright solitons [10–15].

Outside the quasi-1D limit the GPE continues to support bright solitary matter waves. These exhibit many solitonlike characteristics and have been the subject of much experimental [6–8] and theoretical [16–29] investigation. Both bright solitons and bright solitary waves are excellent candidates for use in atom interferometry [30], as their coherence, spatial localization, and solitonlike dynamics offer a metrological advantage in, e.g., the study of atom-surface interactions [7,20]. Toward this end, proposals to phase-coherently split bright solitons and bright solitary waves using a scattering potential [27–29] and an internal state interference protocol [18] and to form soliton molecules [26] have been explored in the literature. However, while the dynamics and collisions of bright solitary waves have been explored in detail and have been shown to be solitonlike in three-dimensional (3D) parameter regimes [16–18], less attention has been directed at the question of exactly how solitonlike the ground state of the system is. In particular, the experimental feasibility of reaching the quasi-1D limit of an attractively interacting BEC, and hence obtaining a highly solitonlike ground state, remains an area lacking a thorough quantitative exploration. Obtaining such a ground state, in addition to being interesting in its own right, would be highly advantageous in experiments seeking to probe quantum effects beyond the mean-field description [27–29], and possibly to exploit the effects of macroscopic quantum superposition to enhance metrological precision [31,32]. Similar concerns regarding adverse residual 3D effects in interferometric protocols prompted a recent perturbative study of residual 3D effects in highly anisotropic, repulsively interacting BECs [33].

The potential instability to collapse of attractively interacting BECs [34–44] is the key obstacle to realizing solitonlike behavior in a BEC. Previous studies of bright solitary-wave dynamics, using variational and numerical solutions of partially quasi-1D GPEs [12,13,21,45] (reductions of the GPE to a 1D equation which retains some 3D character, in contrast to the full quasi-1D limit) and the 3D GPE [16–18,34], have shown the collapse instability to be associated with nonsolitonlike behavior. However, previous studies of bright solitary-wave ground states have focused on identifying the critical parameters at which collapse occurs. Approaches used in these studies include partially quasi-1D methods [12], variational methods [46] using Gaussian [10,34,47] and soliton (sech) [34,48] *Ansätze*, perturbative methods [49], and numerical solutions to the 3D GPE [34,35,43,44,48]. In the last case, the collapse threshold parameters have been extensively mapped out for a range of trap geometries [43,44].

In this paper we use analytic variational and highly accurate numerical solutions of the stationary GPE to systematically and quantitatively assess how solitonlike the ground state of an attractively interacting BEC in a prolate, cylindrically symmetric harmonic trap is, over a wide regime of trap and interaction strengths. Beginning with previously considered variational *Ansätze* based on Gaussian [10,34,47] and soliton [34,48] profiles, we obtain analytic variational solutions for the GPE ground state. Comparison of the soliton-*Ansatz* variational solution to highly accurate numerical solutions of the stationary GPE, which we calculate over an extensive parameter space, gives a quantitative measure of how solitonlike the ground state is. In the regime where the axial and radial trap strengths dominate over the interactions, we show that the Gaussian-*Ansatz* variational solution gives an excellent approximation to the true ground state for all anisotropies;

in this regime the ground state is not solitonlike. In the regime in which the interactions dominate over the axial, but *not* the radial, trap strength, we demonstrate that the soliton-*Ansatz* variational solution does approximate the true, highly solitonlike ground state. However, we show that the goodness of the approximation and the extent of this regime, where it exists at all, are highly restricted by the collapse instability; even at large anisotropies it occupies a narrow window adjacent to the regime where interactions begin to dominate over *all* trap strengths, leading to non-quasi-1D, nonsolitonlike solutions and, ultimately, collapse.

Our results have substantial practical value for experiments using attractively interacting BECs; primarily they define the challenging experimental regime required to realize a highly solitonlike ground state, which would be extremely useful to observe quantum effects beyond the mean-field description, such as macroscopic superposition of solitons [27–29]. We note that bright solitary-wave experiments to date have not reached this regime [6–8]. Secondarily, our quantitative analysis of a wide parameter space provides a picture of the ground state in a wide range of possible attractively interacting BEC experiments. In particular, it indicates the regimes in which a full numerical solution of the 3D GPE is well approximated by one of our analytic variational solutions, which are significantly easier and less time consuming to determine.

The remainder of the paper is structured as follows: After introducing the most general classical field Hamiltonian and stationary GPE in Sec. II, we begin by discussing the quasi-1D limit in Sec. III. In Sec. III A we define the dimensionless trap frequency γ; in the quasi-1D limit this is the *only* free parameter, and all our results are expressed in terms of this quantity. Similarly, our variational *Ansätze* are motivated by the limiting behaviors of the solution in the quasi-1D case; in this case we define them as Gaussian and soliton profiles, parametrized by their axial lengths. In Secs. III B and III C we find, analytically, the energy-minimizing axial lengths for each *Ansatz* as a function of γ. Comparison of the resulting *Ansatz* solutions to highly accurate numerical solutions of the stationary quasi-1D GPE allows us to determine, in the quasi-1D limit, the regimes of low γ in which highly solitonlike ground states can be realized (Sec. III D). We then consider the 3D GPE in Sec. IV. The system then has a second free parameter in addition to γ; we choose this to be κ, the (dimensionless) trap anisotropy, which is defined in Sec. IV A. In Secs. IV B to IV E we define 3D Gaussian and soliton *Ansätze*, adapted from their quasi-1D analogs and each parametrized by an axial and a radial length, and find the energy-minimizing lengths for each *Ansatz*. In general this requires only a very simple numerical procedure, and in the limit of a waveguidelike trap can be expressed analytically (Sec. IV F). In Sec. IV G we compare the *Ansatz* solutions to highly accurate numerical solutions of the stationary 3D GPE and in Sec. IV H assess the potential for realizing truly solitonlike ground states. Finally, Sec. V comprises the conclusions.

II. SYSTEM OVERVIEW

We consider a BEC of N atoms of mass m and (attractive) s-wave scattering length $a_s < 0$, held within a cylindrically symmetric, prolate (the radial frequency ω_r is greater than the axial frequency ω_x) harmonic trap. The ground state is described by the stationary Gross-Pitaevskii equation

$$\left[-\frac{\hbar^2}{2m}\nabla^2 + V(\mathbf{r}) - \frac{4\pi N|a_s|\hbar^2}{m}|\psi(\mathbf{r})|^2 - \lambda \right]\psi(\mathbf{r}) = 0, \tag{1}$$

where the trapping potential $V(\mathbf{r}) = m[\omega_x^2 x^2/2 + \omega_r^2(y^2 + z^2)/2]$, λ is a real eigenvalue, and the Gross-Pitaevskii wave function $\psi(\mathbf{r})$ is normalized to 1. This equation is generated by the classical field Hamiltonian (through the functional derivative $\delta H[\psi]/\delta\psi^* = \lambda\psi$)

$$H[\psi] = \int d\mathbf{r}\left[\frac{\hbar^2}{2m}|\nabla\psi(\mathbf{r})|^2 + V(\mathbf{r})|\psi(\mathbf{r})|^2 - \frac{2\pi N|a_s|\hbar^2}{m}|\psi(\mathbf{r})|^4 \right]. \tag{2}$$

This functional of the classical field ψ describes the total energy per particle, and the ground-state solution minimizes the value of this functional.

When dealing with variational *Ansätze* for the ground-state solution, we proceed by analytically minimizing an energy functional in the same form as Eq. (2) for a given *Ansatz*. In contrast, highly accurate numerical ground states are more conveniently obtained by solving a stationary GPE of the same form as Eq. (1).

III. QUASI-1D LIMIT

A. Reduction to 1D and rescaling

For sufficiently tight radial confinement ($\omega_r \gg \omega_x$), such that the atom-atom interactions are nonetheless essentially 3D [$a_s \ll (\hbar/m\omega_r)^{1/2}$], it is conventional [10–15] to assume a reduction to a quasi-1D stationary GPE

$$\left[-\frac{\hbar^2}{2m}\frac{\partial^2}{\partial x^2} + \frac{m\omega_x^2 x^2}{2} - g_{1D}N|\psi(x)|^2 - \lambda \right]\psi(x) = 0. \tag{3}$$

Typically $\psi(\mathbf{r})$ is taken to be factorized into $\psi(x)$ and the radial harmonic ground state $(m\omega_r/\pi\hbar)^{1/2}\exp(-m\omega_r[y^2 + z^2]/2\hbar)$, such that $g_{1D} = 2\hbar\omega_r|a_s|$. Alternative factorizations are also possible, which lead to an effective 1D equation retaining more 3D character than Eq. (3) [12,13,21,45]; similar factorizations have also been introduced for axially rotating BECs [50] and for quasi-2D BECs in oblate traps [51]. In the absence of the axial harmonic confining potential ($\omega_x \to 0$), there exist exact bright soliton solutions to Eq. (3) of the general form[1]

$$\frac{1}{2b_x^{1/2}}\mathrm{sech}\left(\frac{[x - vt + C]}{2b_x}\right) \times e^{iv(x-vt)m/\hbar}e^{img_{1D}^2N^2t/8\hbar^3}e^{imv^2t/2\hbar}e^{iD}, \tag{4}$$

[1]Equation (4) describes solutions of unit norm. More general soliton solutions $(B/2b_x^{1/2})\mathrm{sech}(B[x - vt + C]/2b_x)$ $e^{iv(x-vt)m/\hbar}e^{iB^2mg_{1D}^2N^2t/8\hbar^3}e^{imv^2t/2\hbar}e^{iD}$ have norm B (and effective mass $\eta = B/4$), such as arise when considering several solitons simultaneously.

where $b_x \equiv \hbar^2/mg_{1D}N$ is a length scale characterizing the soliton's spatial extent, v is the soliton velocity, C is an arbitrary displacement, and D is an arbitrary phase.

This effective 1D Gross-Pitaevskii equation contains two key length scales: the axial harmonic length $a_x \equiv (\hbar/m\omega_x)^{1/2}$ and the soliton length b_x. A mathematically convenient way to express the single free parameter of Eq. (3) is as the square of the ratio of these two length scales;

$$\gamma \equiv \left(\frac{b_x}{a_x}\right)^2 \equiv \frac{\hbar\omega_x}{4m\omega_r^2|a_s|^2N^2}. \tag{5}$$

This parametrization is achieved by working in "soliton units"; lengths are expressed in units of b_x and energies are expressed in units of $mg_{1D}^2N^2/\hbar^2$. This system can be codified as $\hbar = m = g_{1D}N = 1$, and yields the dimensionless quasi-1D GPE

$$\left[-\frac{1}{2}\frac{\partial^2}{\partial x^2} + \frac{\gamma^2x^2}{2} - |\psi(x)|^2 - \lambda\right]\psi(x) = 0, \tag{6}$$

in which γ can be interpreted as a dimensionless trap frequency [15]. The corresponding classical field Hamiltonian is

$$H_{1D}[\psi] = \int dx\left[\frac{1}{2}\left|\frac{\partial}{\partial x}\psi(x)\right|^2 + \frac{\gamma^2x^2}{2}|\psi(x)|^2 - \frac{1}{2}|\psi(x)|^4\right]. \tag{7}$$

The choice of γ for the single free parameter in the 1D GPE [Eq. (6)] and the classical field Hamiltonian [Eq. (7)] can be most directly pictured as choosing to hold the interaction strength constant while varying the axial trap strength, parametrized by γ. Experimentally, however, any of ω_x, ω_r, a_s, and N may be varied in order to vary γ. In the case $\gamma = 0$ the exact ground-state solution is a single, stationary bright soliton: $\psi(x) = \mathrm{sech}(x/2)/2$. In the following sections we develop analytic variational solutions $\psi(x)$ for general γ. Comparison of these solutions to highly accurate numerical solutions of the quasi-1D GPE then gives a picture of the behavior of the ground state with γ. Furthermore, these quasi-1D variational solutions motivate the later 3D variational solutions and yield several mathematical expressions which reappear in the more complex 3D calculations.

B. Variational solution: Gaussian *Ansatz*

We first consider the Gaussian variational *Ansatz*

$$\psi(x) = \left(\frac{\gamma}{\pi\ell_G^2}\right)^{1/4} e^{-\gamma x^2/2\ell_G^2}, \tag{8}$$

where the variational parameter ℓ_G quantifies the axial length. In the trap-dominated limit ($\gamma \to \infty$), the true solution tends to a Gaussian with $\ell_G = 1$. Substituting Eq. (8) into Eq. (7) yields (using identities from Appendix A)

$$H_{1D}(\ell_G) = \frac{\gamma}{4}\left(\ell_G^2 + \frac{1}{\ell_G^2} - \frac{2}{(2\pi\gamma)^{1/2}\ell_G}\right), \tag{9}$$

where H_{1D} is now expressed as a function of the axial length ℓ_G. Setting $\partial H_{1D}/\partial\ell_G = 0$ reveals that the variational energy described by Eq. (9) is minimized when ℓ_G is a positive, real solution to the quartic equation

$$\ell_G^4 + \frac{\ell_G}{(2\pi\gamma)^{1/2}} - 1 = 0. \tag{10}$$

The positive, real solution to this quartic is (see the solution in Appendix B)

$$\ell_G = \frac{[\chi(\gamma)]^{1/2}}{2^{4/3}(\pi\gamma)^{1/6}}\left\{\left[\left(\frac{2}{\chi(\gamma)}\right)^{3/2} - 1\right]^{1/2} - 1\right\}, \tag{11}$$

where we have, for notational convenience, defined χ to have γ dependence such that

$$\chi(\gamma) = \left[1 + \left(1 + \frac{1024\pi^2\gamma^2}{27}\right)^{1/2}\right]^{1/3} + \left[1 - \left(1 + \frac{1024\pi^2\gamma^2}{27}\right)^{1/2}\right]^{1/3}. \tag{12}$$

C. Variational solution: Soliton *Ansatz*

Secondly, we consider a soliton *Ansatz*

$$\psi(x) = \frac{1}{2\ell_S^{1/2}}\mathrm{sech}\left(\frac{x}{2\ell_S}\right), \tag{13}$$

where the variational parameter ℓ_S again quantifies the axial length. In the axially untrapped limit ($\gamma \to 0$), the true solution tends to a classical bright soliton, as described by the above *Ansatz* with $\ell_S = 1$. The variational energy per particle is given by (using identities from Appendix A)

$$H_{1D}(\ell_S) = \frac{\pi^2\gamma^2}{6}\left(\ell_S^2 + \frac{1}{4\pi^2\gamma^2\ell_S^2} - \frac{1}{2\pi^2\gamma^2\ell_S}\right), \tag{14}$$

which is minimized when

$$\ell_S^4 + \frac{\ell_S}{4\pi^2\gamma^2} - \frac{1}{4\pi^2\gamma^2} = 0. \tag{15}$$

Again, this quartic can be solved analytically (see the solution in Appendix B) to give the positive, real minimizing value of ℓ_S:

$$\ell_S = \frac{[\chi(\gamma)]^{1/2}}{2^{11/6}(\pi\gamma)^{2/3}}\left\{\left[\left(\frac{2}{\chi(\gamma)}\right)^{3/2} - 1\right]^{1/2} - 1\right\}, \tag{16}$$

with χ defined as in Eq. (12).

D. Analysis and comparison to 1D numerical solutions

The energy-minimizing axial lengths ℓ_G and ℓ_S, defined by Eqs. (11) and (16) respectively, are shown as functions of γ in Fig. 1(a). There is no collapse instability in the quasi-1D GPE, and solutions are obtained for all (positive, real) γ. As intended by the chosen forms of the *Ansätze*, the limiting cases are $\ell_G \to 1$ as $\gamma \to \infty$ and $\ell_S \to 1$ as $\gamma \to 0$. To evaluate the accuracy of the *Ansätze* for general γ, we compare each *Ansatz* with the numerically determined ground state of the quasi-1D GPE. The computation of a numerically exact ground state $\psi_0(x)$, and the corresponding ground-state energy E_{1D}, uses a pseudospectral method in a basis of symmetric Gauss-Hermite functions; this is a simplified version of the pseudospectral method used for 3D calculations, which is explained in more detail in the next section. Several quantities are compared in Figs. 1(b)–1(d): the variational minimum energies H_{1D} for each *Ansatz* and the numerical ground-state energy E_{1D} are

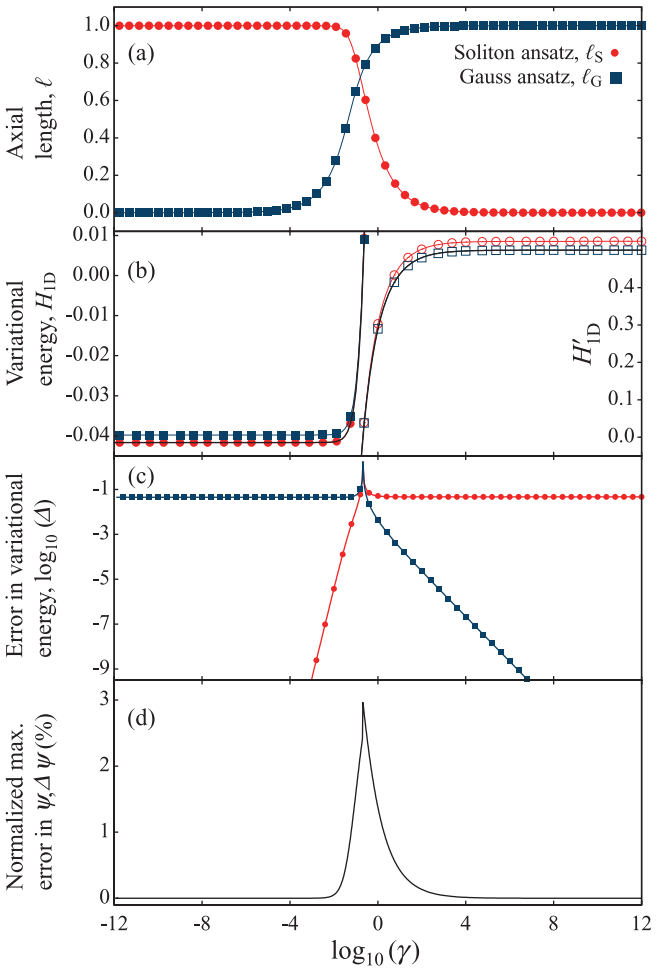

FIG. 1. (Color online) Comparison of quasi-1D variational and numerical solutions: (a) Energy-minimizing axial lengths ℓ_G (Gaussian *Ansatz*, squares) and ℓ_S (soliton *Ansatz*, circles) for the quasi-1D GPE. (b) Minimum variational energy compared with the numerically calculated ground-state energy E_{1D} (black line) for each *Ansatz*: for low γ we show H_{1D} (solid symbols), which tends to $-1/24$ as $\gamma \to 0$; for high γ we show $H'_{1D} = H_{1D}/\gamma$ (hollow symbols), which tends to $1/2$ as $\gamma \to \infty$ (H'_{1D} is equal to the energy expressed in the "harmonic units" $\hbar = m = \omega_x = 1$). (c) Relative error in the variational energy, $\Delta = (H_{1D} - E_{1D})/E_{1D}$. (d) Normalized maximum deformation of the best-fitting *Ansatz* wave function ψ_{Ansatz} with respect to the numerical ground state ψ_0, $\Delta\psi = \max(|\psi_{Ansatz} - \psi_0|)/\max(\psi_0)$, expressed as a percentage. For clarity in (a),(b) [(c)], every 16th [20th] datum is marked by a symbol.

shown in Fig. 1(b); the relative error between H_{1D} and E_{1D}, defined as $\Delta = (H_{1D} - E_{1D})/|E_{1D}|$, is shown for each *Ansatz* in Fig. 1(c); and the maximum difference between the most appropriate *Ansatz* wave function (that with lowest Δ) and the numerical ground-state wave function, expressed as a percentage of the maximum value of the numerically exact ground state, $\Delta\psi = \max(|\psi_{Ansatz} - \psi_0|)/\max(\psi_0)$ [Fig. 1(d)]. All the shown computed quantities are insensitive to a doubling of the numerical basis size from 500 to 1000 states.

Both the Gaussian and soliton *Ansätze* provide an excellent approximation to the exact solutions over a large range of γ. In the regimes where the relative error in the energy Δ becomes significantly lower than 10^{-9} in particular, the difference between the *Ansatz* solutions and numerical solutions becomes generally indistinguishable from numerical round-off error. For the Gaussian *Ansatz* the convergence to this regime is noticeably slower than for the soliton *Ansatz* [Fig. 1(c)]. This effect is a consequence of the parametrization in terms of γ and the corresponding "soliton units": increasing γ leads not only to to higher trap strength, but also to higher peak densities $|\psi(x)|^2$, and hence a stronger nonlinear effect.

For later comparison to the 3D case, it is useful to define a benchmark value of the relative error Δ that indicates excellent agreement between the *Ansatz* and the numerically exact solution. Such a definition, however, will vary according to purpose. As our objectives in this paper relate significantly to the *shape* of the ground state, this forms the basis of our benchmark; a maximum deformation of the wave function below 0.1% of the peak value [as measured by $\Delta\psi$ in Fig. 1(d)] corresponds very closely to $\Delta < 10^{-5}$. Because the relative error Δ saturates to a background value of $\approx 10^{-1}$ in regimes where the chosen *Ansatz* is inapplicable, a value of Δ four orders of magnitude below this background value thus corresponds to an excellent match in shape between the *Ansatz* and the numerically exact solution. With respect to this benchmark, the Gaussian *Ansatz* represents an excellent fit for $\log_{10}(\gamma) > 1.15$, while the ground state is highly solitonlike (the soliton *Ansatz* represents an excellent fit) for $\log_{10}(\gamma) < -0.95$.

IV. BRIGHT SOLITARY-WAVE GROUND STATES IN 3D

A. Rescaling to effective 1D soliton units

We now consider the cylindrically symmetric 3D Gross-Pitaevskii equation [Eq. (1)]. Compared to the quasi-1D effective Gross-Pitaevskii equation [Eq. (6)], three-dimensionality introduces an additional relevant length scale, the radial harmonic length $a_r = (\hbar/m\omega_r)^{1/2}$. We incorporate this into the dimensionless trap anisotropy $\kappa \equiv \omega_r/\omega_x$, which forms an additional free parameter. Expressed in the same "soliton units" as Eq. (6), Eq. (1) becomes

$$\left[-\frac{1}{2}\nabla^2 + V(\mathbf{r}) - \frac{2\pi}{\kappa\gamma}|\psi(\mathbf{r})|^2 - \lambda\right]\psi(\mathbf{r}) = 0, \qquad (17)$$

with corresponding energy functional

$$H_{3D}[\psi] = \int d\mathbf{r}\left[\frac{1}{2}\nabla\psi(\mathbf{r})\cdot\nabla\psi^*(\mathbf{r}) + V(\mathbf{r})|\psi(\mathbf{r})|^2 - \frac{\pi}{\kappa\gamma}|\psi(\mathbf{r})|^4\right], \qquad (18)$$

where $V(\mathbf{r}) = \gamma^2[x^2 + \kappa^2(y^2 + z^2)]/2$.

In the following sections we obtain variational solutions for general κ and γ using *Ansätze* similar to the Gaussian and soliton *Ansätze* employed in the previous section, with an additional variable-width Gaussian radial profile. Contrary to the case in the quasi-1D limit, a self-consistent energy-minimizing solution for both the axial and radial length parameters cannot be expressed entirely analytically. However, we reduce the numerical work required to the simultaneous solution of two equations and introduce a straightforward iterative technique to achieve this. We also consider the case of a waveguidelike trap ($\omega_x = 0$) separately, where an entirely

analytic variational solution exists (Sec. IV F). Subsequently, in Sec. IV G, we again compare the *Ansatz* solutions to high-accuracy numerics.

B. Variational solution: Gaussian *Ansatz*

We first consider an *Ansatz* composed of Gaussian axial and radial profiles. We phrase this as

$$\psi(\mathbf{r}) = \frac{\kappa^{1/2}\gamma^{3/4}k_{\mathrm{G}}}{\pi^{3/4}\ell_{\mathrm{G}}^{1/2}} e^{-\kappa\gamma k_{\mathrm{G}}^2(y^2+z^2)/2} e^{-\gamma x^2/2\ell_{\mathrm{G}}^2}. \tag{19}$$

Here, the first variational parameter ℓ_{G} quantifies the axial length of the *Ansatz* in analogy to the quasi-1D case. The *reciprocal* of the second variational parameter, k_{G}^{-1}, quantifies the radial length of the *Ansatz*. In the trap-dominated limit ($\gamma \to \infty$) both these lengths approach unity ($\{\ell_{\mathrm{G}}, k_{\mathrm{G}}\} \to 1$). Substitution of this *Ansatz* into Eq. (18) yields (using identities from Appendix A)

$$H_{3\mathrm{D}}(\ell_{\mathrm{G}}, k_{\mathrm{G}}) = \frac{\gamma}{4}\left(\ell_{\mathrm{G}}^2 + \frac{1}{\ell_{\mathrm{G}}^2} - \frac{2k_{\mathrm{G}}^2}{(2\pi\gamma)^{1/2}\ell_{\mathrm{G}}} + 2\kappa k_{\mathrm{G}}^2 + \frac{2\kappa}{k_{\mathrm{G}}^2}\right). \tag{20}$$

Setting the partial derivatives with respect to both ℓ_{G} and k_{G} equal to zero, we deduce that ℓ_{G} must solve the quartic equation

$$\ell_{\mathrm{G}}^4 + \frac{k_{\mathrm{G}}^2\ell_{\mathrm{G}}}{(2\pi\gamma)^{1/2}} - 1 = 0, \tag{21}$$

and that k_{G} must solve

$$k_{\mathrm{G}} = \left(\frac{(2\pi\gamma)^{1/2}\kappa\ell_{\mathrm{G}}}{(2\pi\gamma)^{1/2}\kappa\ell_{\mathrm{G}} - 1}\right)^{1/4}. \tag{22}$$

From Eq. (22) it follows that we must have $\ell_{\mathrm{G}} > 1/(2\pi\gamma)^{1/2}\kappa$ to obtain a physically reasonable solution, i.e., a real, positive value of k_{G}, consistent with our initial *Ansatz*. For a given such value of k_{G}, Eq. (21) is solved (see the solution in Appendix B) by

$$\ell_{\mathrm{G}} = \frac{\left[\chi\left(\gamma k_{\mathrm{G}}^{-4}\right)\right]^{1/2}k_{\mathrm{G}}^{2/3}}{2^{4/3}(\pi\gamma)^{1/6}}\left\{\left[\left(\frac{2}{\chi\left(\gamma k_{\mathrm{G}}^{-4}\right)}\right)^{3/2} - 1\right]^{1/2} - 1\right\}, \tag{23}$$

with χ defined as in Eq. (12).

C. Analysis of Gaussian-*Ansatz* solution

Contrary to the quasi-1D limit, minimization of the variational energy in 3D requires simultaneous solution of two equations for the radial length k_{G}^{-1} and the axial length ℓ_{G}. These equations are, respectively, Eq. (22) and [rearranged from Eq. (21)]

$$k_{\mathrm{G}} = \left[\frac{(2\pi\gamma)^{1/2}}{\ell_{\mathrm{G}}}\left(1 - \ell_{\mathrm{G}}^4\right)\right]^{1/2}. \tag{24}$$

These equations dictate that physical solutions must have

$$\frac{1}{(2\pi\gamma)^{1/2}\kappa} < \ell_{\mathrm{G}} < 1, \tag{25}$$

and hence that $\gamma > 1/2\pi\kappa^2$ must be satisfied in order for physical solutions to exist.

Where solutions exist, they must be found numerically. However, a very practical method of numerical solution follows from the shape of the ℓ_{G} surface defined by Eq. (23), and shown in Fig. 2(a), which is a decreasing function of k_{G} for all (real, positive) γ. The method can be considered graphically, in terms of locating the intersection(s) of Eqs. (22) and (24). These curves are shown, for various κ, in Figs. 2(b)–2(d), along with the lower bound from inequality (25). Below a κ-dependent threshold value of γ the curves fail to intersect, indicating instability of the BEC to collapse. At the threshold value [dotted curves in Figs. 2(b)–2(d)] there is exactly one intersection, and above the threshold value [the other curves in Figs. 2(b)–2(d)] there are two intersections. In the latter case the higher-ℓ_{G} intersection, which smoothly deforms to the limiting case $\{\ell_{\mathrm{G}}, k_{\mathrm{G}}\} \to 1$ as $\gamma \to \infty$, represents the physical, minimal-energy variational solution. This solution can be located using a simple "staircase" method: substitution of a trial value $\bar{k}_{\mathrm{G}}$, satisfying $1 \leqslant \bar{k}_{\mathrm{G}} < k_{\mathrm{G}}$, into Eq. (23) produces a trial value $\bar{\ell}_{\mathrm{G}}$ satisfying $\ell_{\mathrm{G}} < \bar{\ell}_{\mathrm{G}} \leqslant 1$, and subsequent substitution of this trial value into Eq. (22) produces an iterated trial value $\bar{k}'_{\mathrm{G}}$ satisfying $\bar{k}_{\mathrm{G}} < \bar{k}'_{\mathrm{G}} < k_{\mathrm{G}}$. Thus, beginning with $\bar{k}_{\mathrm{G}} = 1$, iteration of this process converges the trial values to the true k_{G} and ℓ_{G}.

The physical solutions to Eqs. (21) and (22) for different anisotropies κ are shown on the ℓ_{G} surface, and projected into the ℓ_{G}-γ plane, in Fig. 2(a). These solutions are also shown as black crosses in the ℓ_{G}-k_{G} plane in Figs. 2(b)–2(d), where they form a line connecting the physical-solution intersections of Eqs. (22) and (24) for the various γ shown. In Fig. 2(a) the collapse instability is manifest as a rapid rise in k_{G}—corresponding to a decrease in radial extent—and fall in ℓ_{G}—corresponding to a decrease in axial extent—just above a κ-dependent threshold value of γ. There are no self-consistent solutions for these quantities below this collapse threshold. For increasing anisotropies κ, this collapse threshold occurs at lower values of γ. For the highest two values of κ considered the collapse threshold lies in the regime where ℓ_{G} is already approaching 0; our analysis of the Gaussian *Ansatz* in the quasi-1D limit indicates that the 3D Gaussian *Ansatz* will be a poor approximation to the true solution in this regime. Importantly, for γ above the collapse threshold the projected curves for each anisotropy agree well with the Gaussian *Ansatz* in the quasi-1D GPE, suggesting that the Gaussian *Ansatz* gives a good approximation to the true solution here.

D. Variational solution: Soliton *Ansatz*

Second, we consider a soliton *Ansatz* composed of an axial sech profile and a radial Gaussian profile. We phrase this as

$$\psi(\mathbf{r}) = \frac{\gamma^{1/2}\kappa^{1/2}k_{\mathrm{S}}}{(2\pi\ell_{\mathrm{S}})^{1/2}} e^{-\kappa\gamma k_{\mathrm{S}}^2(y^2+z^2)/2}\mathrm{sech}(x/2\ell_{\mathrm{S}}). \tag{26}$$

As with the 3D Gaussian *Ansatz*, the first variational parameter ℓ_{G} quantifies the axial length of the *Ansatz* and the *reciprocal* of the second variational parameter, k_{G}^{-1}, quantifies its radial length. In the quasi-1D limit both lengths consequently approach unity ($\{\ell_{\mathrm{G}}, k_{\mathrm{G}}\} \to 1$). Substitution of this *Ansatz* into Eq. (18) yields (using identities from Appendix A)

$$H_{3\mathrm{D}}(\ell_{\mathrm{S}}, k_{\mathrm{S}}) = \frac{\pi^2\gamma^2}{6}\left(\ell_{\mathrm{S}}^2 + \frac{1}{4\pi^2\gamma^2\ell_{\mathrm{S}}^2} - \frac{k_{\mathrm{S}}^2}{2\pi^2\gamma^2\ell_{\mathrm{S}}} + \frac{3\kappa k_{\mathrm{S}}^2}{\pi^2\gamma} + \frac{3\kappa}{\pi^2\gamma k_{\mathrm{S}}^2}\right). \tag{27}$$

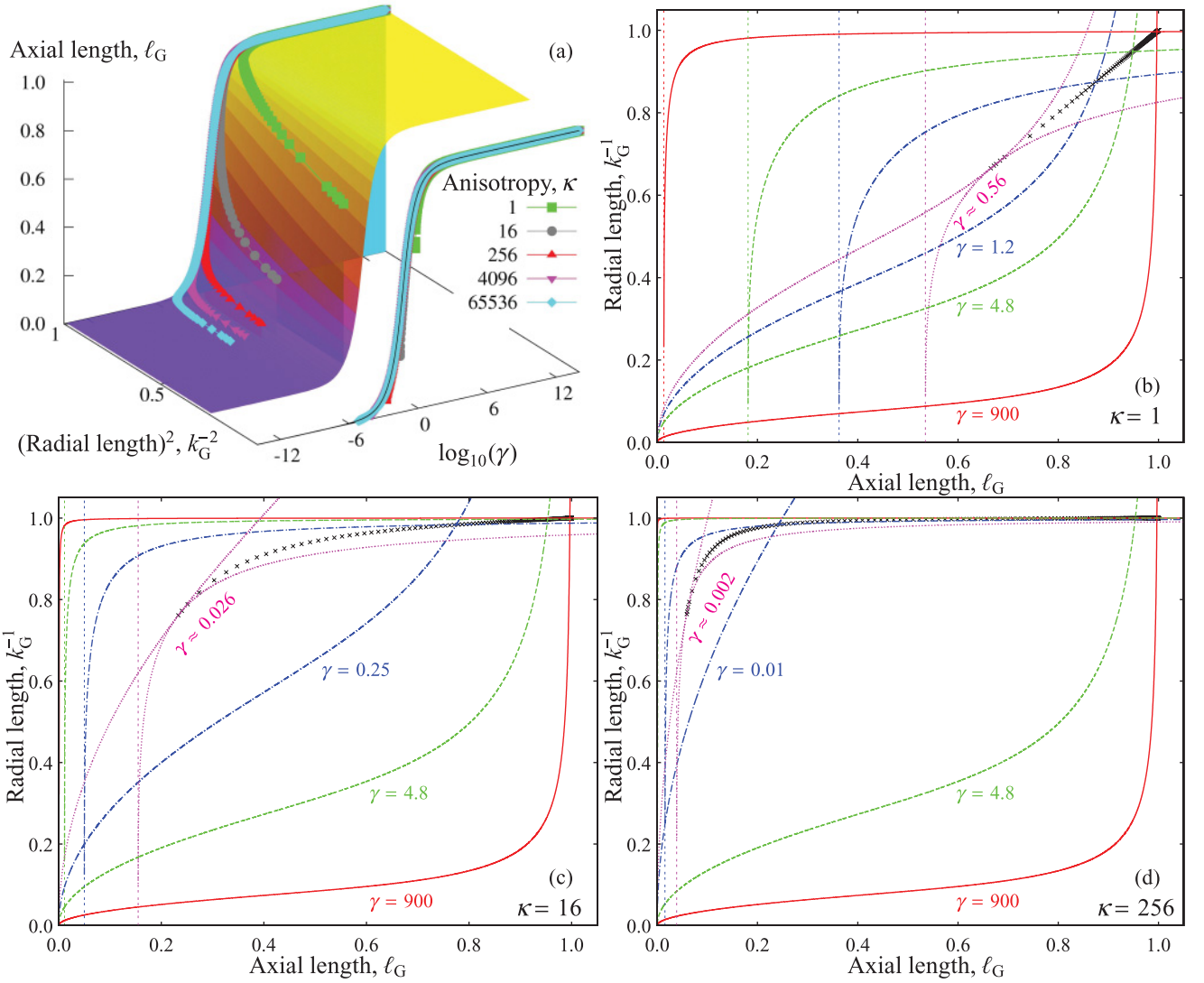

FIG. 2. (Color online) Energy-minimizing variational parameters for the 3D GPE using a Gaussian *Ansatz*: (a) axial length ℓ_G as a function of the radial length k_G^{-1} and the parameter γ [Eq. (23)]. Lines show the simultaneous solutions of Eqs. (22) and (24) for the axial length ℓ_G and radial length k_G^{-1}, for different anisotropies κ and values of γ. Projections of these solutions on the γ-ℓ_G plane are also shown; here the black line indicates the quasi-1D result [from Fig. 1(a)]. (b)–(d) Illustration of the intersections of Eqs. (22) [lines with vertical asymptote $\ell_G = 1/(2\pi\gamma)^{1/2}\kappa$ shown with fine dashes] and (24) for various κ: the higher-ℓ_G intersection, which corresponds to a physical solution for the axial length ℓ_G and radial length k_G^{-1}, can be found using a "staircase" method starting from $k_G = 1$. The numerical solutions obtained in this way, and shown by points in (a), are shown by crosses in (b)–(d). The lowest values of γ plotted in (b)–(d) are the lowest for which a self-consistent Gaussian *Ansatz* solution is found.

Once again, setting partial derivatives with respect to both ℓ_S and k_S equal to zero allows us to deduce that

$$\ell_S^4 + \frac{k_S^2 \ell_S}{4\pi^2\gamma^2} - \frac{1}{4\pi^2\gamma^2} = 0, \tag{28}$$

and that k_S must solve

$$k_S = \left(\frac{6\kappa\gamma\ell_S}{6\kappa\gamma\ell_S - 1}\right)^{1/4}. \tag{29}$$

From Eq. (29) it follows that we must have $\ell_S > 1/6\kappa\gamma$ to obtain a physically reasonable solution, i.e., a real, positive value of k_S, consistent with our initial *Ansatz*. For a given such value of k_S, Eq. (28) is solved (see the solution in Appendix B) by

$$\ell_S = \frac{\left[\chi\left(\gamma k_S^{-4}\right)\right]^{1/2} k_S^{2/3}}{2^{11/6}(\pi\gamma)^{2/3}} \left\{\left[\left(\frac{2}{\chi\left(\gamma k_S^{-4}\right)}\right)^{3/2} - 1\right]^{1/2} - 1\right\}, \tag{30}$$

with χ defined as in Eq. (12).

E. Analysis of soliton-*Ansatz* solution

As in the case of the Gaussian *Ansatz*, minimization of the variational energy in 3D requires the simultaneous solution of equations for the radial length k_S^{-1} and the axial length ℓ_S.

These equations are, respectively, Eq. (29) and [rearranged from Eq. (28)]

$$k_S = \left[\frac{1}{\ell_S}\left(1 - 4\pi^2\gamma^2\ell_S^4\right)\right]^{1/2}. \tag{31}$$

These equations dictate that physical solutions must have

$$\frac{1}{6\kappa\gamma} < \ell_S < \frac{1}{(2\pi\gamma)^{1/2}} \tag{32}$$

and hence that $\gamma > (\pi/3)^2/2\pi\kappa^2$ must be satisfied in order for physical solutions to exist. These equations and constraints can be further simplified by casting them in terms of $\ell_S' = (2\pi\gamma)^{1/2}\ell_S$; this yields two equations,

$$k_S = \left(\frac{(2\pi\gamma)^{1/2}\kappa\ell_S'}{(2\pi\gamma)^{1/2}\kappa\ell_S' - \pi/3}\right)^{1/4} \tag{33}$$

and

$$k_S = \left[\frac{(2\pi\gamma)^{1/2}}{\ell_S'}\left(1 - \ell_S'^4\right)\right]^{1/2}, \tag{34}$$

and an inequality,

$$\frac{\pi/3}{(2\pi\gamma)^{1/2}\kappa} < \ell_S' < 1, \tag{35}$$

which are extremely similar to those encountered in the case of the Gaussian *Ansatz*. The numerical solution of these equations for the physical solution, which can exist only when $\gamma > (\pi/3)^2/2\pi\kappa^2$, follows the same procedure as used for the Gaussian *Ansatz*.

Variational-energy-minimizing solutions to the soliton-*Ansatz* equations for different anisotropies κ are shown in Fig. 3; these are shown superimposed on the ℓ_S surface and projected into the ℓ_S-γ plane in Fig. 3(a), and alongside Eqs. (28) and (29) and inequality (35) in Figs. 3(b)–3(d). The collapse instability is even more evident in the soliton *Ansatz* than in the Gaussian *Ansatz*, since it occurs in a region with a larger background value of ℓ_S. Once again, the collapse is manifest as a rapid rise in k_S and drop in ℓ_S—corresponding to both axial and radial contraction of the solution—immediately prior to a κ-dependent threshold value of γ. Below the threshold, no self-consistent solutions exist. For increasing anisotropies κ, this collapse threshold again occurs at lower values of γ. In contrast to the case of the Gaussian *Ansatz*, however, the collapse instability precludes solutions in exactly the limit where one expects the soliton *Ansatz* to be accurate ($\gamma \to 0$). This property of the collapse instability severely restricts the possibility of observing highly bright-soliton-like ground states in 3D. The solution curves in Fig. 3(a) illustrate that this effect is worst for low trap anisotropies κ, but is to some extent mitigated for higher κ. However, a full comparison with numerically exact solutions is necessary to quantify these effects; we undertake such a comparison in Sec. IV G.

F. Variational solution: Waveguide configuration

In broad experimental terms, the collapse instability sets a maximum value for the ratio of interaction strength to trap strength (equivalent to a minimum value of γ) which increases (and hence the minimum value of γ decreases) with the trap anisotropy κ. In the context of atomic BEC experiments one would typically think of controlling γ by varying either $|a_s|$ or N while holding ω_r and ω_x constant; in this situation the collapse instability places a trap-anisotropy-dependent upper limit on the product $|a_s|N$. However, the minimum value of γ does not increase without limit in the trap anisotropy κ: In an experiment one can, in principle, remove all axial trapping to create a waveguidelike configuration; in this case $\omega_x = 0$ and the trap anisotropy $\kappa \to \infty$, while the parameter $\gamma \to 0$. In this limit a reparametrization is necessary, and only needs to be performed for the soliton *Ansatz*, which is clearly more appropriate in this context.

Elimination of the axial trap removes one of the two free parameters of the 3D GPE [Eq. (17)]. The remaining free parameter is $\Gamma = \gamma\kappa = (a_r/2|a_s|N)^2$, where $a_r = (\hbar/m\omega_r)^{1/2}$ is the radial harmonic oscillator length scale. The soliton *Ansatz* may be rewritten in terms of Γ as

$$\psi(\mathbf{r}) = \frac{\Gamma^{1/2}k_S}{(2\pi\ell_S)^{1/2}}e^{-\Gamma k_S^2(y^2+z^2)/2}\mathrm{sech}(x/2\ell_S). \tag{36}$$

Substituting this into Eq. (18) with $\omega_x = 0$ yields (using identities from Appendix A),

$$H_{3D}(\ell_S, k_S) = \left(\frac{1}{24\ell_S^2} - \frac{k_S^2}{12\ell_S} + \frac{\Gamma k_S^2}{2} + \frac{\Gamma}{2k_S^2}\right), \tag{37}$$

from which we deduce that the energy-minimizing variational parameters satisfy

$$\ell_S = \frac{1}{k_S^2} \tag{38}$$

and

$$k_S = \left(\frac{6\Gamma\ell_S}{6\Gamma\ell_S - 1}\right)^{1/4}. \tag{39}$$

Contrary to the more general 3D case, an analytic simultaneous solution of Eqs. (38) and (39) exists when ℓ_S satisfies the depressed cubic equation

$$\ell_S^3 - \ell_S + \frac{1}{6\Gamma} = 0. \tag{40}$$

Using the general solution for a depressed cubic equation from Appendix B, one finds that the physical root (with real, positive ℓ_S satisfying the limit $\ell_S \to 1$ as $\Gamma \to \infty$) is given by

$$\ell_S = \left[-\frac{1}{12\Gamma} + \frac{1}{3^{3/2}\Gamma}\left(\frac{3}{16} - \Gamma^2\right)^{1/2}\right]^{1/3} + \left[-\frac{1}{12\Gamma} - \frac{1}{3^{3/2}\Gamma}\left(\frac{3}{16} - \Gamma^2\right)^{1/2}\right]^{1/3}. \tag{41}$$

Consequently, solutions exist only for $\Gamma > 3^{1/2}/4$, as shown in Fig. 4(a).

G. Comparison to 3D numerical solutions

The variational-energy-minimizing axial lengths ℓ_G and ℓ_S are shown as functions of γ in Fig. 5(a) for the general 3D case; for the waveguide limit both axial and radial lengths ℓ_S and k_S^{-1} are shown as functions of Γ in Fig. 4(a). As in

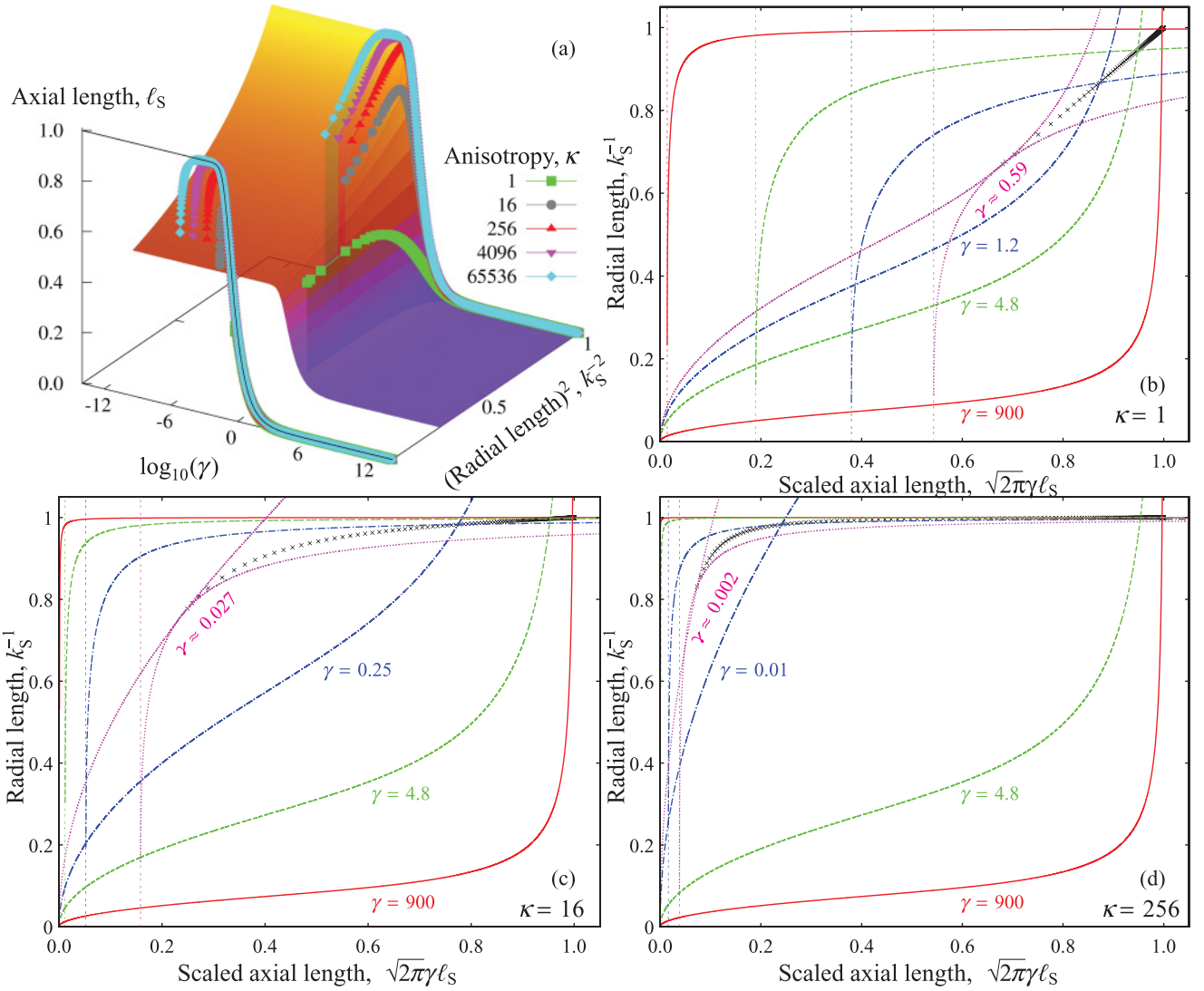

FIG. 3. (Color online) Energy-minimizing variational parameters for the 3D GPE using a soliton *Ansatz*: (a) axial length ℓ_S as a function of the radial length k_S^{-1} and the parameter γ [Eq. (30)]. Lines show the simultaneous solutions of Eqs. (33) and (34) for the axial length ℓ_S and radial length k_S^{-1}, for different anisotropies κ and values of γ. Projections of these solutions on the γ-ℓ_S plane are also shown; here the black line indicates the quasi-1D result [from Fig. 1(a)]. (b)–(d) Illustration of the intersections of Eqs. (33) [lines with vertical asymptote $\ell_S = (\pi/3)/(2\pi\gamma)^{1/2}\kappa$ shown with fine dashes] and (34) for various κ: the higher-ℓ_S intersection, which corresponds to a physical solution for the axial length ℓ_S and radial length k_S^{-1}, can be found using a staircase method starting from $k_S = 1$. The numerical solutions obtained in this way, and shown by points in (a), are shown by crosses in (b)–(d). The lowest values of γ plotted in (b)–(d) are the lowest for which a self-consistent soliton *Ansatz* solution is found.

the quasi-1D case, we quantitatively evaluate the accuracy of the *Ansatz* solutions for general γ (Γ) by comparing the variational minimum energy H_{3D} with the numerically determined ground-state energy E_{3D}. We calculate E_{3D} using a pseudospectral method in a basis of optimally scaled harmonic oscillator eigenstates; this is formed from a tensor product of symmetric Gauss-Hermite functions (axial direction) and generalized Laguerre functions (radial direction). The *Ansatz* with the lowest variational energy is used both to optimize the scaling of the basis functions and as an initial estimate for the solution. Expanding the stationary 3D GPE in such a basis produces a system of nonlinear equations which are solved iteratively using a modified Newton method. A similar method was used to solve a similar cylindrically symmetric, stationary 3D GPE, with repulsive interactions, in Ref. [52].

As in the quasi-1D case, we compare several quantities between the *Ansatz* and numerical solutions. Figure 5(b) shows the *scaled* energy $H'_{3D} = (H_{3D}/\gamma)/(1 + 1/2\kappa)$ in the general 3D case. This scaling is such that E'_{3D}—which is defined analogously to H'_{3D} with respect to E_{3D}—tends to 1 as $\gamma \to \infty$. Figures 5(c) and 5(d) show the relative error in the variational minimum energy $\Delta = (H_{3D} - E_{3D})/E_{3D}$ for the Gaussian and soliton *Ansätze*, respectively. The same quantity Δ is shown for the waveguide limit in Fig. 4(b). All quantities shown in Figs. 4 and 5 are computed using between 2000 and 12 000 basis states (κ dependent) and are insensitive to a doubling of the number of basis states.

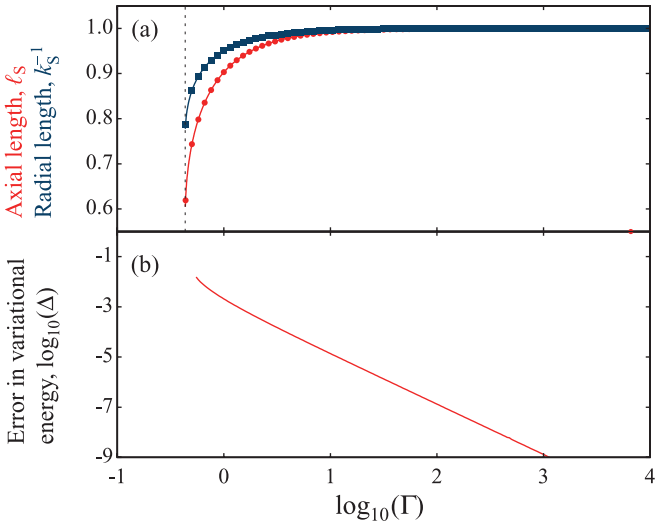

FIG. 4. (Color online) Comparison of 3D variational and numerical solutions in a waveguide configuration ($\omega_x = 0$): (a) Energy-minimizing axial length ℓ_S and radial length k_S^{-1} for the soliton *Ansatz*. Solutions, given by Eq. (41), exist for all $\Gamma = \kappa\gamma > 3^{1/2}/4$. (b) Relative error in the minimum variational energy of the soliton *Ansatz*, $\Delta = (H_{3D} - E_{3D})/E_{3D}$, where E_{3D} is the numerically determined ground-state energy.

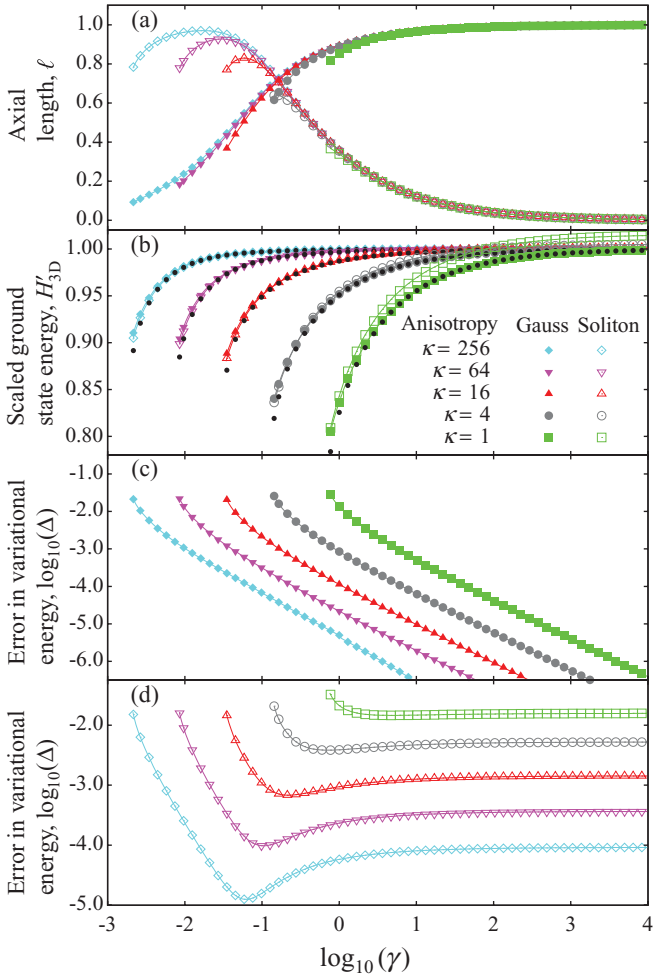

FIG. 5. (Color online) Comparison of 3D variational and numerical solutions: (a) Energy-minimizing axial lengths ℓ_G (Gaussian *Ansatz*, solid symbols) and ℓ_S (soliton *Ansatz*, hollow symbols). (b) Scaled variational energies $H'_{3D} = \kappa H_{3D}/\gamma(\kappa + 1/2)$ [a similarly scaled ground-state energy $E'_{3D} = \kappa E_{3D}/\gamma(\kappa + 1/2)$ tends to 1 in the limit $\gamma \to \infty$ for all anisotropies κ] compared with the numerically calculated ground-state energies E_{3D} (black dots). (c),(d) Normalized relative error in the variational energy $\Delta = (H_{3D} - E_{3D})/E_{3D}$ for the Gaussian (c) and soliton (d) *Ansätze*. For clarity every fourth datum is marked by a symbol in (a)–(d).

In the general 3D case, a close inspection of Figs. 5(b)–5(d) is necessary to reveal the overall relation between the *Ansatz* solutions and the numerically obtained ground state. In the high-γ limit, Fig. 5(b) shows that both the Gaussian variational energies (solid symbols) and the ground-state energy E_{3D} (black dots) approach 1 as $\gamma \to \infty$, whereas the soliton-*Ansatz* energies (hollow symbols) tend to higher energies. This corresponds to the actual ground state most closely matching the Gaussian *Ansatz* in this limit, as one would expect. Indeed, the relative error in variational energy, Δ, for the Gaussian *Ansatz* [Fig. 5(c)] continues to drop exponentially with γ for all anisotropies κ, making it possible to find regimes of γ where the Gaussian *Ansatz* gives an excellent approximation to the true ground state.

In the opposite, low-γ limit, collapse occurs at a κ-dependent value of γ; this corresponds to the points in Figs. 5(a)–5(d) where solution curves abruptly cease. Prior to collapse (at higher values of γ) the relation between the Gaussian *Ansatz*, the soliton *Ansatz*, and the actual ground state is highly dependent on the trap anisotropy κ [Fig. 5(b)]. In the case of a spherically symmetric trap, where the anisotropy $\kappa = 1$, the soliton-*Ansatz* variational energy is *never* closer to the true ground-state energy E_{3D} than the Gaussian-*Ansatz* variational energy. A regime of solitonlike ground states consequently cannot exist at this low anisotropy; as the soliton *Ansatz* is intrinsically asymmetric, this is to be expected. For higher anisotropies, the soliton-*Ansatz* energy is closer to E_{3D} than the Gaussian-*Ansatz* energy in a small regime prior to collapse. Exactly how solitonlike the ground state is in this regime can be quantitatively assessed using the relative error Δ. This is shown for the soliton *Ansatz* in Fig. 5(d). For each κ the "background" value of Δ in the limit $\gamma \to \infty$ is different; this effect is due to the decreasing size of the axial part of the energy with respect to the radial part for increasing γ. In the opposite, low-γ, limit Δ increases sharply close to the collapse point as the ground-state wave function rapidly contracts. The maximum extent to which Δ decreases from its high-γ limit *before* this increase, due to collapse-related contraction at low γ, quantifies how solitonlike the ground state becomes in this regime. Even for the highest anisotropy shown, $\kappa = 256$, the regime of γ over which Δ drops below its background value is rather narrow, and the actual drop in Δ is only one order of magnitude. Compared to the benchmark of Sec. III D, this indicates that the true ground state remains considerably deformed with respect to the soliton *Ansatz*. The minimum error in the soliton-*Ansatz* energy does, however, improve with increasing anisotropy κ. Excellent agreement can be achieved in the waveguide limit ($\kappa \to \infty$): Fig. 4 shows

that excellent agreement, with respect to the benchmark figure of Sec. III D, can be obtained for $\Gamma > 10^{3/2}$.

H. Discussion

A physical interpretation of the above results follows from considering two conditions that must be satisfied in order to realize a solitonlike ground state: (1) the radial profile should be "frozen" to a Gaussian, thus realizing a quasi-1D limit; and (2) interactions should dominate over the axial trapping. On first inspection these conditions seem mutually compatible and satisfiable simply by increasing the radial trap frequency ω_r with other parameters held constant. However, condition (1) can be satisfied only if the maximum density remains low enough to avoid any deformation of the radial profile due to the collapse instability. Increasing ω_r leads to exactly such deformation, and ultimately to collapse, as it has the secondary effect of strongly increasing the density. This strong increase in density with ω_r is particular to the case of attractive interactions. Increasing ω_r in a repulsively interacting BEC likewise acts to increase the density, but this increase is counteracted by the interactions; these act to reduce the density and cause the BEC to expand axially. In the attractively interacting case the response of the interactions is the opposite: increasing ω_r leads to axial *contraction* of the BEC. Consequently condition (1) is far harder to satisfy for an attractively interacting BEC than for a repulsively interacting one. Responding to this problem simply by reducing the interaction strength (either through $|a_s|$ or N) leads to violation of condition (2). The nature of the problem is made particularly clear by considering the waveguide limit: here condition (2) is automatically satisfied ($\omega_x = 0$). This makes it possible to achieve a highly solitonlike ground state by satisfying condition (1) alone. However, such a ground state is achieved by *lowering* the product $\omega_r^{1/2}|a_s|N$, and thus by progressing toward the limit of extreme diluteness.

This physical behavior of the system presents considerable challenges for experiments aiming to realize a highly solitonlike ground state. In essence, the most desirable configuration is to have extremely high anisotropies κ while keeping ω_r as low as possible. Realization of such a configuration through extremely low, or zero, axial trap frequencies ω_x is problematic: such frequencies are hard to set precisely experimentally as they require a very smooth potential to be generated, potentially over a considerable length. Furthermore, in the case $\omega_x = 0$ the mean-field approximation ceases to be valid for an attractively interacting BEC; the true wave function should be translationally invariant in this case, but the mean-field solution breaks this symmetry [53]. Even for very low but nonzero ω_x the mean-field approximation can lose validity due to the extreme diluteness of the BEC, and the energy gap from the ground state to states with excited axial modes can become low enough to cause significant population of the excited states at experimentally feasible temperatures.

It is informative to consider the parameters used in bright solitary-wave experiments to date [6–8]. None of these aimed to realize highly solitonlike ground states in the sense considered here. However, they nonetheless indicate regimes which have proved to be experimentally accessible and offer a guide to future possibilities. All have operated outside the regime of highly solitonlike ground states; direct comparison of the experiments of Refs. [7,8] with our results reveals that κ is too small in these experiments ($\kappa \approx 11$ and $\kappa \approx 3$ respectively) to achieve a highly solitonlike ground state. The experiment of Ref. [6] featured an expulsive axial potential, which does not yield a value of κ suitable for direct comparison with our results. However, it is possible to assume the waveguide limit $\omega_x = 0$ in each experiment and compare the values of Γ with our results: in each case $\Gamma \lesssim 1$, outside the regime of highly solitonlike ground states. Thus, experiments with weaker traps and lower densities than previously realized with attractive condensates appear to be necessary in order to achieve a highly solitonlike ground state.

V. CONCLUSIONS

In this paper we considered attractively interacting atomic BECs in cylindrically symmetric, prolate harmonic traps, and introduced variational *Ansätze*, based on Gaussian and bright-soliton profiles, for the GPE ground state. We compared analytic variational solutions based on these *Ansätze* with highly accurate numerical solutions of the GPE over an extensive parameter space, and hence determined how solitonlike the ground state is. Initially assuming the quasi-1D limit to be valid, we showed that the true solution to the GPE is (not) solitonlike when interactions do (not) dominate over the trap strength. In 3D, this picture is complicated by the collapse instability; in the regime where all trap strengths dominate over the interactions a Gaussian variational *Ansatz* gives an excellent approximation to the true, and non-soliton-like, ground state. In contrast to the quasi-1D limit, however, we have shown that the regime in which the ground state is truly solitonlike (well approximated by a soliton variational *Ansatz*) is either nonexistent, or highly restricted, depending on the trap anisotropy. For low anisotropies, as one raises the strength of the interactions such that they approach and exceed the strength of the axial trap, the true ground state ceases to be well described by a Gaussian variational *Ansatz*, but does not become well described by a soliton variational *Ansatz* before the interaction strength also exceeds the radial trapping strength, leading to collapse. Only by raising the anisotropy significantly can one open a parameter window in which the true ground state becomes solitonlike before the interaction strength is sufficient to cause collapse.

Our results describe the nature of the ground state over a wide parameter regime and offer a straightforward, accurate approximation to the full 3D GPE solution in many cases. Our results are particularly relevant for experiments using attractively interacting condensates as they identify the potentially challenging parameter regime required to observe a truly solitonlike ground state, which would be an advantageous regime for experiments seeking to explore and exploit beyond-mean-field effects such as a macroscopic superposition of bright solitons. Given that previous studies have shown that the dynamics and collisions of bright solitary waves can be solitonlike over a much wider parameter regime than our approach reveals the ground state to be, extension of the

variational approach used here to dynamical situations is an interesting direction for future work.

ACKNOWLEDGMENTS

We thank S. L. Cornish, D. I. H. Holdaway, H. Salman, and C. Weiss for discussions, and the U.K. EPSRC (Grant No. EP/G056781/1), the Jack Dodd Centre (S.A.G.), and Durham University (T.P.B.) for support.

APPENDIX A: USEFUL INTEGRALS

Considering a Gaussian *Ansatz* to be proportional to $e^{-k^2x^2}$, for completeness we reprise the following sequence of well-known integral identities, all of which are necessary to determine the corresponding variational energy functional:

$$\int_{-\infty}^{\infty} dx\, e^{-2k^2x^2} = \frac{\sqrt{\pi/2}}{k} \Rightarrow \int_{-\infty}^{\infty} dx\, e^{-4k^2x^2} = \frac{\sqrt{\pi}}{2k}, \tag{A1}$$

$$\int_{-\infty}^{\infty} dx\, x^2 e^{-2k^2x^2} = -\frac{1}{4k}\frac{\partial}{\partial k}\int_{-\infty}^{\infty} dx\, e^{-2k^2x^2} = \frac{\sqrt{\pi/2}}{4k^3}, \tag{A2}$$

$$\int_{-\infty}^{\infty} dx \left(\frac{\partial}{\partial x} e^{-k^2x^2}\right)^2 = 4k^4 \int_{-\infty}^{\infty} dx\, x^2 e^{-k^2x^2} = k\sqrt{\pi/2}. \tag{A3}$$

Comparable integral identities exist when considering an *Ansatz* proportional to $\mathrm{sech}(kx)$. Thus:

$$\int_{-\infty}^{\infty} dx\, \mathrm{sech}^2(kx) = \left[\frac{\tanh(kx)}{k}\right]_{-\infty}^{\infty} = \frac{2}{k}, \tag{A4}$$

$$\int_{-\infty}^{\infty} dx\, \mathrm{sech}^4(kx) = \left[\frac{\{\mathrm{sech}^2(kx)+2\}\tanh(kx)}{3k}\right]_{-\infty}^{\infty} = \frac{4}{3k}, \tag{A5}$$

$$\int_{-\infty}^{\infty} dx \left[\frac{\partial}{\partial x}\mathrm{sech}(kx)\right]^2 = k^2 \int_{-\infty}^{\infty} dx\, \tanh^2(kx)\mathrm{sech}^2(x) = \frac{k}{3}[\tanh(kx)]_{-\infty}^{\infty} = \frac{2k}{3}, \tag{A6}$$

all of which are necessary to determine the energy of a standard bright soliton solution to the nonlinear Schrödinger equation. However, we also require a contribution arising from the existence of an external harmonic confining potential. Hence, we determine

$$\begin{aligned}\int_{-\infty}^{\infty} dx\, x^2\mathrm{sech}^2(kx) &= 2\int_0^{\infty} dx\, x^2\mathrm{sech}^2(kx)\\ &= \frac{2}{k^3}[\mathrm{Li}_2(-e^{-2kx}) + kx\{kx\tanh(kx)\\ &\quad - kx - 2\ln(1+e^{-2kx})\}]_0^{\infty}\\ &= \frac{2}{k^3}[\mathrm{Li}_2(0) - \mathrm{Li}_2(-1)]\\ &= \frac{2}{k^3}\eta(2) = \frac{\pi^2}{6k^3},\end{aligned} \tag{A7}$$

where $\mathrm{Li}_y(x) \equiv \sum_{n=1}^{\infty} x^n/n^y$ is a polylogarithm, and $-\mathrm{Li}_y(-1) = \eta(y)$ the Dirichlet η function, with $\eta(2) = \pi^2/12$.

APPENDIX B: SOLUTION TO THE QUARTIC EQUATIONS

We require a general solution to a quartic in ℓ of the form

$$\ell^4 + b\ell - c = 0, \tag{B1}$$

where b and c are positive real constants, and ℓ must also take positive real values to be physically meaningful. This can be rephrased as the product of two quadratics in ℓ:

$$\left[\ell^2 + \alpha\ell + \frac{1}{2}\left(\alpha^2 - \frac{b}{\alpha}\right)\right]\left[\ell^2 - \alpha\ell + \frac{1}{2}\left(\alpha^2 + \frac{b}{\alpha}\right)\right] = 0, \tag{B2}$$

so long as $(b^2/\alpha^2 - \alpha^4)/4 = c$. Hence, α, which remains to be determined, must solve $\alpha^6 + 4c\alpha^2 - b^2$.

Defining $\xi = \alpha^2$, the problem of determining α reduces to finding values of ξ to solve the depressed cubic equation

$$\xi^3 + 4c\xi - b^2 = 0. \tag{B3}$$

Defining

$$A = \sqrt[3]{\frac{b^2}{2} + \sqrt{\frac{b^4}{4} + \frac{64c^3}{27}}}, \quad B = \sqrt[3]{\frac{b^2}{2} - \sqrt{\frac{b^4}{4} + \frac{64c^3}{27}}}, \tag{B4}$$

the three roots of Eq. (B3) are given by

$$\xi_1 = A + B, \tag{B5}$$

$$\xi_2 = -(A+B)/2 + i\sqrt{3}(A-B)/2, \tag{B6}$$

$$\xi_3 = -(A+B)/2 - i\sqrt{3}(A-B)/2. \tag{B7}$$

Any one of these will solve Eq. (B3), however we choose ξ_1; as b and c are assumed positive real, ξ_1 is also conveniently guaranteed positive real.

Substituting in $\alpha = \sqrt{\xi_1}$, we can apply the quadratic formula to both the factors (enclosed in square brackets) on the left-hand side of Eq. (B2). This reveals the four roots to be

$$\ell_1 = \frac{-\sqrt{\xi_1} + \sqrt{-\xi_1 + 2b/\sqrt{\xi_1}}}{2}, \tag{B8}$$

$$\ell_2 = \frac{-\sqrt{\xi_1} - \sqrt{-\xi_1 + 2b/\sqrt{\xi_1}}}{2}, \tag{B9}$$

$$\ell_3 = \frac{\sqrt{\xi_1} + \sqrt{-\xi_1 - 2b/\sqrt{\xi_1}}}{2}, \tag{B10}$$

$$\ell_4 = \frac{\sqrt{\xi_1} - \sqrt{-\xi_1 - 2b/\sqrt{\xi_1}}}{2}. \tag{B11}$$

Recalling that b and ξ_1 are positive real, ℓ_3 and ℓ_4 are clearly complex, and therefore not of interest to us. Noting that

$$\xi_1^3 = A^3 + B^3 + 3AB(A+B) = b^2 - 4c\xi_1, \tag{B12}$$

we can see that $A^3 + B^3 \equiv b^2 > \xi_1^3$; hence $4b^2 > \xi_1^3$ and thus $2b/\sqrt{\xi_1} > \xi_1$. Roots ℓ_1 and ℓ_2 are therefore real, but ℓ_2 is guaranteed negative. However, from Eq. (B12) it also follows that

$$\begin{aligned} b > \xi_1\sqrt{\xi_1} &\Rightarrow 2b/\sqrt{\xi_1} > 2\xi_1 \Rightarrow 2b/\sqrt{\xi_1} - \xi_1 > \xi_1\\ &\Rightarrow \sqrt{-\xi_1 + 2b/\sqrt{\xi_1}} > \sqrt{\xi_1}. \end{aligned} \tag{B13}$$

Hence ℓ_1 is guaranteed positive real and is the only solution of interest.

Thus, the single positive real root of Eq. (B1) is

$$\ell = \frac{\chi^{1/2} b^{1/3}}{2^{7/6}} \left\{ \left[\left(\frac{2}{\chi} \right)^{3/2} - 1 \right]^{1/2} - 1 \right\}, \tag{B14}$$

with

$$\chi = \left\{ 1 + \left[1 + \frac{(c/3)^3}{(b/4)^4} \right]^{1/2} \right\}^{1/3} + \left\{ 1 - \left[1 + \frac{(c/3)^3}{(b/4)^4} \right]^{1/2} \right\}^{1/3}, \tag{B15}$$

and where values of all fractional powers are taken to be real, and positive when a positive root exists.

[1] T. Dauxois and M. Peyrard, *Physics of Solitons* (Cambridge University Press, Cambridge, 2006).
[2] L. D. Fadeev and L. A. Takhtajan, *Hamiltonian Methods in the Theory of Solitons* (Springer-Verlag, Berlin, 1987).
[3] V. E. Zakharov and A. B. Shabat, Zh. Eksp. Theor. Fiz. **61**, 118 (1971) [Sov. Phys. JETP **34**, 62 (1972)].
[4] J. Satsuma and N. Yajima, Prog. Theor. Phys. Suppl. **55**, 284 (1974).
[5] J. P. Gordon, Opt. Lett. **8**, 596 (1983).
[6] L. Khaykovich, F. Schreck, G. Ferrari, T. Bourdel, J. Cubizolles, L. D. Carr, Y. Castin, and C. Salomon, Science **296**, 1290 (2002).
[7] K. E. Strecker, G. B. Partridge, A. G. Truscott, and R. G. Hulet, Nature (London) **417**, 150 (2002).
[8] S. L. Cornish, S. T. Thompson, and C. E. Wieman, Phys. Rev. Lett. **96**, 170401 (2006).
[9] L. Pitaevskii and S. Stringari, *Bose-Einstein Condensation* (Clarendon Press, Oxford, 2003).
[10] V. M. Pérez-García, H. Michinel, J. I. Cirac, M. Lewenstein, and P. Zoller, Phys. Rev. Lett. **77**, 5320 (1996).
[11] V. M. Pérez-García, H. Michinel, and H. Herrero, Phys. Rev. A **57**, 3837 (1998).
[12] L. Salasnich, A. Parola, and L. Reatto, Phys. Rev. A **65**, 043614 (2002).
[13] L. Salasnich, A. Parola, and L. Reatto, Phys. Rev. A **66**, 043603 (2002).
[14] A. D. Martin, C. S. Adams, and S. A. Gardiner, Phys. Rev. Lett. **98**, 020402 (2007).
[15] A. D. Martin, C. S. Adams, and S. A. Gardiner, Phys. Rev. A **77**, 013620 (2008).
[16] N. G. Parker, A. M. Martin, S. L. Cornish, and C. S. Adams, J. Phys. B **41**, 045303 (2008).
[17] N. G. Parker, A. M. Martin, C. S. Adams, and S. L. Cornish, Physica D **238**, 1456 (2009).
[18] T. P. Billam, S. L. Cornish, and S. A. Gardiner, Phys. Rev. A **83**, 041602(R) (2011).
[19] D. Poletti, E. A. Ostrovskaya, T. J. Alexander, B. Li, and Y. S. Kivshar, Physica D **238**, 1338 (2009).
[20] S. L. Cornish, N. G. Parker, A. M. Martin, T. E. Judd, R. G. Scott, T. M. Fromhold, and C. S. Adams, Physica D **238**, 1299 (2009).
[21] L. Khaykovich and B. A. Malomed, Phys. Rev. A **74**, 023607 (2006).
[22] U. Al Khawaja, H. T. C. Stoof, R. G. Hulet, K. E. Strecker, and G. B. Partridge, Phys. Rev. Lett. **89**, 200404 (2002).
[23] K. E. Strecker, G. B. Partridge, A. G. Truscott, and R. G. Hulet, New J. Phys. **5**, 73 (2003).
[24] L. D. Carr and J. Brand, Phys. Rev. Lett. **92**, 040401 (2004).
[25] B. J. Dąbrowska-Wüster, S. Wüster, and M. J. Davis, New J. Phys. **11**, 053017 (2009).
[26] U. Al Khawaja and H. T. C. Stoof, New J. Phys. **13**, 085003 (2011).
[27] C. Weiss and Y. Castin, Phys. Rev. Lett. **102**, 010403 (2009).
[28] A. I. Streltsov, O. E. Alon, and L. S. Cederbaum, Phys. Rev. Lett. **99**, 030402 (2007).
[29] A. I. Streltsov, O. E. Alon, and L. S. Cederbaum, Phys. Rev. A **80**, 043616 (2009).
[30] A. D. Cronin, J. Schmiedmayer, and D. E. Pritchard, Rev. Mod. Phys. **81**, 1051 (2009).
[31] J. A. Dunningham and K. Burnett, Phys. Rev. A **70**, 033601 (2004).
[32] J. A. Dunningham, Contemp. Phys. **47**, 257 (2006).
[33] A. B. Tacla and C. M. Caves, Phys. Rev. A **84**, 053606 (2011).
[34] N. G. Parker, S. L. Cornish, C. S. Adams, and A. M. Martin, J. Phys. B **40**, 3127 (2007).
[35] P. A. Ruprecht, M. J. Holland, K. Burnett, and M. Edwards, Phys. Rev. A **51**, 4704 (1995).
[36] J. L. Roberts, N. R. Claussen, S. L. Cornish, E. A. Donley, E. A. Cornell, and C. E. Wieman, Phys. Rev. Lett. **86**, 4211 (2001).
[37] E. A. Donley, N. R. Claussen, S. L. Cornish, J. L. Roberts, E. A. Cornell, and C. E. Wieman, Nature (London) **412**, 295 (2001).
[38] J. M. Gerton, D. Strekalov, I. Prodan, and R. G. Hulet, Nature (London) **408**, 692 (2000).
[39] R. J. Dodd, M. Edwards, C. J. Williams, C. W. Clark, M. J. Holland, P. A. Ruprecht, and K. Burnett, Phys. Rev. A **54**, 661 (1996).
[40] L. P. Pitaevskii, Phys. Lett. A **221**, 14 (1996).
[41] C. M. Savage, N. P. Robins, and J. J. Hope, Phys. Rev. A **67**, 014304 (2003).
[42] P. A. Altin, G. R. Dennis, G. D. McDonald, D. Döring, J. E. Debs, J. D. Close, C. M. Savage, and N. P. Robins, Phys. Rev. A **84**, 033632 (2011).
[43] A. Gammal, T. Frederico, and L. Tomio, Phys. Rev. A **64**, 055602 (2001).
[44] A. Gammal, L. Tomio, and T. Frederico, Phys. Rev. A **66**, 043619 (2002).
[45] A. M. Kamchatnov and V. S. Shchesnovich, Phys. Rev. A **70**, 023604 (2004).
[46] B. A. Malomed, Prog. Opt. **43**, 71 (2002).
[47] V. M. Pérez-García, H. Michinel, J. I. Cirac, M. Lewenstein, and P. Zoller, Phys. Rev. A **56**, 1424 (1997).
[48] L. D. Carr and Y. Castin, Phys. Rev. A **66**, 063602 (2002).
[49] V. I. Yukalov and E. P. Yukalova, Phys. Rev. A **72**, 063611 (2005).
[50] L. Salasnich, B. A. Malomed, and F. Toigo, Phys. Rev. A **76**, 063614 (2007).
[51] L. Salasnich and B. A. Malomed, Phys. Rev. A **79**, 053620 (2009).
[52] S. A. Morgan, Phys. Rev. A **72**, 043609 (2005).
[53] Y. Lai and H. A. Haus, Phys. Rev. A **40**, 854 (1989).